Soil & Tillage Research 264 (2026) 107354

Contents lists available at ScienceDirect

Soil & Tillage Research

journal homepage: www.elsevier.com/locate/still

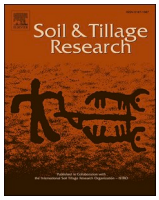

# High resolution 4D soil organic carbon stock mapping at farm scale

Nícolas Augusto Rosin [a,b], José A.M. Demattê [a,c,*], Heidy Soledad Rodríguez-Albarracín [a], Jorge Tadeu Fim Rosas [a,d], Bruno dos Anjos Bartsch [a], Jean Jesus Macedo Novais [a,b], Marcelo Henrique Procópio Pelegrino [a], Carlos Eduardo Pellegrino Cerri [a,c], Danilo César de Mello [a], Renan Falcioni [e]

[a] Department of Soil Science, Luiz de Queiroz College of Agriculture, University of São Paulo, Pádua Dias Av., 11, Piracicaba, Postal Box 09, São Paulo 13416-900, Brazil
[b] Brazilian Agricultural Research Corporation (Embrapa) –Soils, Rio de Janeiro, RJ 22460-000, Brazil
[c] Center for Carbon Research in Tropical Agriculture (CCARBON), University of São Paulo (USP), Piracicaba São Paulo, Brazil
[d] Department of Agronomy, College of Agricultural Sciences, São Paulo Western University (UNOESTE), Raposo Tavares Hwy, Km 572, Presidente Prudente, São Paulo 19067-175, Brazil
[e] Department of Agronomy, State University of Maringá, Av. Colombo, 5790, Maringá, Paraná 87020-900, Brazil

ARTICLE INFO

*Keywords:*
Pedometrics
Soil health
Digital soil mapping, spatio-temporal mapping

ABSTRACT

Soil organic carbon (SOC) is intrinsically linked to global carbon balance, climate change mitigation, soil health, and agricultural productivity. Therefore, obtaining accurate information on the spatial-temporal of the soil organic carbon stock (SOCS) is essential. We proposed a four-dimensional (4D) SOCS mapping approach, encompassing space (two dimensions), depth and time. A 100 × 100 m grid sampling was conducted in 1997 and 2022 at two depths (0–20 cm and 80–100 cm) in a sugarcane farm. Dynamic and static covariates representing the soil formation processes were used to fit three Cubist models. We tested three strategies for SOCS spatial-temporal mapping: 1) a model for each year, 2) a model fitted using only the data of the last year (2022) and 3) a multitemporal model using data of both periods. Based on external validation, strategy 1 and 3 produced more accurate and less biased maps, with coefficient of determination ($R^2$) of 0.74, root mean square error (RMSE) of 7.69 ton $ha^{-1}$ and bias of 3.43 ton $ha^{-1}$ and $R^2$ of 0.76, RMSE of 7.19 ton $ha^{-1}$ and Bias of 3.25 ton $ha^{-1}$ for strategy 3, respectively. Strategy 2 was less efficient ($R^2 = 0.71$; RMSE = 11.06 ton $ha^{-1}$; Bias = 7.93 ton $ha^{-1}$). Strategy 3 is particularly useful for SOCS mapping when only limited temporal observations are available. Soil attributes (static) were most important covariates for modeling, followed by a bare soil image (dynamic) and vegetation information (dynamic). An increase in SOCS was observed in most sampling sites and predicted maps. The SOCS dynamic was related to soil type, geology and showed an inverse relationship with bare soil frequency. Finally, the SOCS saturation deficit was assessed by spatio-temporal mapping.

## 1. Introduction

Soil organic carbon (SOC) represents two-thirds of the total terrestrial carbon, accounting for approximately 50–80% (Padarian et al., 2022; Stockmann et al., 2013) Given this extensive storage capacity, small changes in SOC can affect atmospheric $CO_2$, concentration and, consequently, global climate (Lal, 2016; Minasny et al., 2017; Zhang et al., 2024). In summary, SOC is intrinsically linked to global carbon balance, climate change mitigation, soil health, and agricultural productivity (Evangelista et al., 2024; Feeney et al., 2024; Hoffland et al., 2020; Liptzin et al., 2022; Wiesmeier et al., 2019). However, due to natural and anthropogenic factors, such as socioeconomic development and land use changes including agriculture and urbanization, SOC shows considerable spatio-temporal variability (Stockmann et al., 2013; Tayebi et al., 2021; Wiesmeier et al., 2019). Therefore, it is essential to obtain accurate information on SOC spatio-temporal variations and to

* Corresponding author at: Department of Soil Science, Luiz de Queiroz College of Agriculture, University of São Paulo, Pádua Dias Av., 11, Piracicaba, Postal Box 09, São Paulo 13416-900, Brazil.
*E-mail addresses:* nicolas.rosin@embrapa.br (N.A. Rosin), jamdemat@usp.br (J.A.M. Demattê), hsrodrigueza@usp.br (H.S. Rodríguez-Albarracín), jorge.fimrosas@usp.br (J.T.F. Rosas), brunobartsch@usp.br (B.A. Bartsch), jean.novais@embrapa.br (J.J.M. Novais), marcelopelegrino@usp.br (M.H.P. Pelegrino), cepcerri@usp.br (C.E.P. Cerri), daniloc.demello@usp.br (D.C. Mello), rfalcioni2@uem.br (R. Falcioni).

https://doi.org/10.1016/j.still.2026.107354
Received 27 May 2025; Received in revised form 18 June 2026; Accepted 26 June 2026
Available online 30 June 2026

understand the predominant factors driving them (Heuvelink et al., 2021; Zhang et al., 2024).

Digital soil mapping (DSM) is an efficient method for spatial prediction of SOC over different scales using a relatively small number of sampling points and environmental covariates (McBratney et al., 2003). There has been an exponential increase in publications of content/stock SOC mapping by DSM and remote sensing in the last two decades. Many SOC maps have been produced at the local or farm level at detailed scales, allowing the use of SOC information for better soil management (Castaldi et al., 2023; Tran et al., 2024; Zhou et al., 2022). Other studies have reached regional, national, and global levels (Adhikari et al., 2014; Gomes et al., 2019; Hengl et al., 2017; Kempen et al., 2019). In parallel, other studies have gone further by mapping other SOC characteristics, such as fractions, dynamic, maximum potential, and deficit of sequestration (Rodríguez-Albarracín et al., 2023, 2024; Román Dobarco et al., 2023). Among these, Rodríguez-Albarracín et al. (2023) mapped the maximum theory potential of SOC sequestration, and the saturation deficit based on soil mineralogy information.

However, most SOC mapping initiatives are static and do not represent SOC temporal variations (Rosin et al., 2026). Unlike conventional DSM, which uses only static soil observation point and covariates, SOC stock (SOCS) spatial-temporal mapping incorporates dynamic covariates over time and soil observation points collected in different periods to capture SOC temporal variations (Heuvelink et al., 2021). This approach allows the derivation of SOC maps beyond the period in which SOC observations are made, based on the assumption that the relationship between SOC and covariates can be extrapolated over time. The accuracy of spatial-temporal DSM machine learning models is largely influenced by the number and distribution of soil observation points in space and time, as well as by the ability of selected dynamic covariates to capture the SOC variations over time (Heuvelink et al., 2021).

Several studies have been developed in that direction. Heuvelink et al. (2021) mapped the SOCS of Argentina between 1982 and 2017 at 0–30 cm depth, using a machine learning multitemporal model (a single model for all periods) and the normalized difference vegetation index (NDVI) as a dynamic covariate. Ugbaje et al. (2024) also used a machine learning multitemporal model with NDVI and climate date as dynamic covariates to predict the SOCS at 0–30 cm depth for Australia between 1990 and 2018. Bartsch et al. (2025) predicted the SOC content from 2014 to 2021 at 0–20 cm depth in an agricultural area in Brazil using points collected in different locations, employing both a multitemporal model and different models for each period. Nguemezi et al. (2021) predicted the SOCSs at reginal scale in Cameroon for 1985 and 2017 at 0–30 cm depth, using different sampling points and different models for each year. In the same way. Similarly, Szatmári et al. (2019) mapped SOCS change between 1992 and 2010 for Hungary at 0–30 cm depth by fitting separate DSM models for both years but using points in collected in the same location.

Most studies use legacy soil data with soil samples collected in different periods, but not in the exact same locations, employing multitemporal models or a different model for each period. According to Heuvelink et al. (2021), repeated measurements over time at the same locations could favor the modeling of temporal change, as well as the inclusion of more relevant covaries to capture SOCS dynamics. In this context, we tested different strategies to SOCS spatio-temporal mapping. We revisited a study area with the first soil sampling grid established in 1997 and re-collected the samples at the same positions and depths in 2022, to verify SOC variation. We also obtained covariates with strong correlation with SOCS, such as soil mineralogy (static) and soil reflectance (dynamic).

We proposed a 4D SOCS mapping approach, encompassing space (two dimensions), depth, and time. We aimed to test three strategies for SOCS spatial-temporal mapping: 1) a separate model for each year; 2) a model fitted using only the data of the last year (2022); and 3) a multitemporal model using data of both periods. We evaluated the extrapolation capacity of models for locations and periods without samples, as well as the importance of environmental covariates in each strategy. We also identified the factors affecting SOCS variations and calculated the SOC saturation and deficit for both periods, based on the study by Rodríguez-Albarracín et al. (2023).

## 2. Material and methods

We tested three different strategies for 4D SOCS temporal mapping. The flowchart of methodology can be found in Fig. 1a.

### 2.1. Study area and soil samples

The study was conducted in a 184 ha sugarcane farm in Rafard, São Paulo, Brazil, located within Peripheral Depression of São Paulo in the Capivari River watershed (Fig. 1b). The lithology is composed of alluvial deposits, diabase, metamorphosed siltstones and siltstones (Nanni, 2000). The climate (Köppen classification) is subtropical mesothermal (Cwa), with an average annual precipitation of 1200 mm and average temperatures of 24 °C (Alvares et al., 2013). The altitudes vary from 474.83 m to 567.69 m and the maximum slope is 35% (Farr and Kobrick, 2000). The study area has a high soil variability, including Cambisols, Gleysols, Chernozens, Nitisols, Lixisols and Leptosols (Bazaglia Filho et al., 2013; IUSS Working Group WRB, 2015).

The study was carried out in an area that has been used for research for a long time. The first soil sampling was conducted in 1997 by Nanni (2000), when a 100 × 100 m grid was demarcated with high precision. At that time, a total of 184 points were sampled using an auger at depths of 0–20 cm and 80–100 cm. In 2022, the points were revisited using a high precision GPS (SP60 GNSS Trimble RTX) and soil sampling was repeated at 119 point locations for each layer. Sampling was not possible at some points due to severe anthropogenic alterations, such as road and terrace construction. It total, we used 119 points from 1997 and 2022 for model calibration, and the 42 points collected exclusively in 1997 were used as an external validation dataset (Fig. 1b). Twenty-three points from the original grid were not used in this study because they are located outside sugarcane areas or outside the SySI image coverage (described below).

For laboratory analyses, the soil samples were air-dried, ground, and passed through a 2 mm sieve. The soil organic carbon (SOC) was determined by the Walkley-Black oxidation method (Walkley and Black,

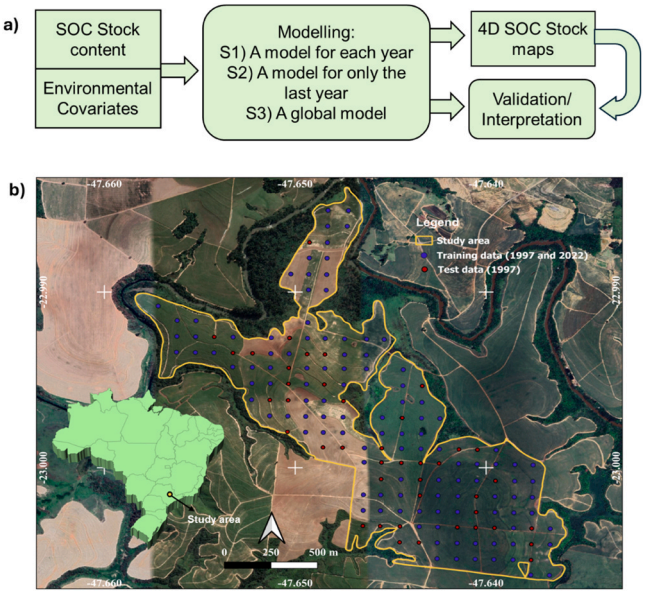


**Fig. 1.** Flowchart of the methodology, study area and sampling points.

1934) and the clay content was determined by the densimeter method (Bouyoucos, 1962). The bulk density (BD) was estimated using a pedotransfer function developed by Benites et al. (2007) for tropical soils: BD (g $cm^3$) = 1.5688 – (0.0005 x clay (g $kg^{-1}$)) – (0.0090 x SOC (g $kg^{-1}$)). Finally, the SOCS was calculated by: SOCS (ton $ha^{-1}$) = SOC (g $kg^{-1}$) x BD (g $cm^{-3}$) x t (cm) / 10, being the layer thickness (t) = 20 cm.

### 2.2. Environmental covariates

In digital soil mapping (DSM), the environmental covariates represent some factors of SCORPAN model (McBratney et al., 2003). In temporal DSM mapping, the covariates can be divided into two groups: static and dynamic. The statics covariates do not change during the study period, explaining only the spatial variations and, in some cases, variations with depth. On the other hand, the dynamic covariates show temporal variation during the study period and explain variations in space and time. The list of environmental covariates is presented in Table 1.

**Table 1**
Environmental covariates list.

| Type | SCORPAN | Predictor name | Source /Reference |
|---|---|---|---|
| Static | Relief | Elevation<br>Slope<br>Northness<br>Eastness<br>Horizontal Curvature<br>Vertical curvature<br>Shape index | SRTM (Farr and Kobrick, 2000) and TAGEE (Safanelli et al., 2020) |
| | Soil** | Clay | (Mendes et al., 2021b) |
| | | Aluminum XRF<br>Iron XRF<br>Silicon XRF | (Rosin et al., 2024) |
| | | Goethite DRS<br>Hematite DRS<br>Kaolinite DRS<br>Gibssite DRS | (Mendes et al., 2021a) |
| Dynamic* | Organisms | NDVI | (Rouse et al., 1973) |
| | | MVeg blue (450–520 nm)<br>MVeg green (520–600 nm)<br>MVeg red (630–690 nm)<br>MVeg NIR (760–900 nm)<br>MVeg SWIR1 (1550–1750 nm)<br>MVeg SWIR2 (2080–2350 nm) | (Rosas et al., 2024) |
| | Soil, PM and time | SYSI blue (450–520 nm)<br>SYSI green (520–600 nm)<br>SYSI red (630–690 nm)<br>SYSI NIR (760–900 nm)<br>SYSI SWIR1 (1550–1750 nm)<br>SYSI SWIR2 (2080–2350 nm) | GEOS3 (Demattê et al., 2018) |
| | Soil and climate | LST | (Ermida et al., 2020) |
| | Time and soil | Auxiliar 1997/0–20 cm<br>Auxiliar 1997/ 80–100 cm<br>Auxiliar 2022/0–20 cm<br>Auxiliar 2022/ 80–100 cm | - |

Where: PM = parent material; XRF = X-ray fluorescence; DRS = diffuse reflectance spectroscopy; NDVI = normalized difference vegetation index; MVeg = maximum vegetation; NIR = near infrared; SWIR = short wave infrared; SYSI = bare soil image; LST = land surface temperature; SRTM = Shuttle Radar Topography Mission; TAGEE = Terrain Analyses in Google Earth Engine; GEOS3 = Geospatial soil Sensing System. * The dynamic covariates were obtained for two periods: 1997–1998 and 2022–2023. ** The soil attributes maps were generated for the layers 0–20 cm and 80–100 cm.

We used static covariates including relief attributes and soil attributes maps. The relief attributes were derived from Shuttle Radar Topography Mission (SRTM) (Farr and Kobrick, 2000) using the Terrain Analyses in Google Earth Engine (TAGEE) (Gorelick et al., 2017; Safanelli et al., 2020). The clay maps were spatialized by Mendes et al. (2021b) by DSM. The chemical elements maps (aluminum, iron and silicon) were obtained by X-ray fluorescence and spatialized by DSM (Rosin et al., 2024). The mineralogical maps (goethite, hematite, kaolinite and gibbsite) were obtained by diffuse reflectance spectroscopy and spatialized by DSM (Mendes et al., 2021a). The soil attributes maps were generated for 0–20 cm and 80–100 cm layers.

The dynamic covariates were derived from different Landsat satellites (5, 7, 8 and 9) for two periods 1997–1998 and 2022–2023 using the Google Earth Engine (Gorelick et al., 2017). First, the Landsat images were normalized and corrected according to Roy et al. (2016a), (2016b). The normalized difference vegetation index (NDVI) (Rouse et al., 1973) was calculated. A maximum vegetation image (MVeg), which is a filtered image containing only vegetation pixels, was generated according to Rosas et al. (2024). A bare soil image (SYSI), which is a filtered image containing only bare soil pixels, was generated according to Demattê et al. (2018). Both MVeg and SYSI have the six Landsat bands: blue, red, green, near infrared, short wave infrared 1 and short-wave infrared 2. A land surface temperature (LST) image was generated according to Ermida et al. (2020). Additionally, four "auxiliar" covariates were created, each one consisting of a categorical image with a single pixel value, where: 1 = 1997 and 0–20 cm; 2 = 1997 and 80–100 cm; 3 = 2022 and 0–20 cm; 4 = 2022 and 80–100 cm.

The resulting environmental covariates have a spatial resolution of 30 m. They were aligned using the "Alling raster" tool and extracted to the training soil points dataset using the "Point Sampling Tool" in the QGIS software (QGIS Development Team, 2024).

### 2.3. Modelling, mapping and validation

Three prediction models were fitted: 1) Model 1: 1997 model, using only points from 1997 and covariates from 1997 to 1998, 2) Model 2: 2022 model, using only points from 2022 and covariates from 2022 to 2023 and 3) Model 3: a multitemporal model, using all dataset points (both 1997 and 2022) and covariates from 1997 to 1998 and 2022–2023. The models were used for predicting SOCS for covariates from 1997 to 1998 and 2022–2023, depending on the strategy tested. In strategy 1, Model 1 was used to predict the SOCS for 1997–1998 covariates, and Model 2 was used to predict SOCS for 2022–2023 covariates. In strategy 2, Model 2 was used to predict the SOCS for both 1997–1998 and 2022–2023 periods. Finally, in strategy 3, Model 3 was used to predict SOCS for both 1997–1998 and 2022–2023 covariates. The maps were obtained for the 0–20 cm and 80–100 cm layers.

The models were built using the Cubist algorithm (Quinlan, 1992) implemented in *caret* R package (Kuhn et al., 2021; R Core Team, 2024). A 5-fold cross-validation (CV) was used to assess the accuracy of the prediction models, and the metrics used were the coefficient of determination ($R^2$), root mean square error (RMSE), and ratio of performance to interquartile distance (RPIQ). The importance of independent variables and the model's rules were reported based on Model 3.

### 2.4. External validation

The maps generated using the three strategies for 1997 and for the 0–20 cm and 80–100 cm layers were sampled at the test dataset (42 points from 1997) using the "Point Sampling Tool" in QGIS software (QGIS Development Team, 2024). The predicted SOCS values were compared with the measured values based on $R^2$, RMSE, and Bias metrics. External validation was the criterion used to decide which was the best strategy.

### 2.5. Data interpretation

The 1997 and 2022 maps obtained using the best strategy (as described in 2.4) for the 0–20 cm and 80–100 cm layers were used in the following analyses. In addition, the SOCS difference map (2022 SOCS – 1997 SOCS) was calculated.

The methodology of Demattê et al. (2020) was used to obtain four maps of bare soil frequency (BSF), which revel how many times bare soil occurred in relation to the total number of pixels in an image time series. The BSF maps were obtained for the periods of two years (1997–1998 and 2022–2023) and for 10 years (1990–2002 and 2010–2022) using GEE (Gorelick et al., 2017). The relationship between BSF and the SOCS and SOCS difference maps was evaluated visually and by Person correlation. Person correlation was performed using the stats R package (R Core Team, 2024).

A detailed geological map was obtained from Nanni (2000), while an ultra-detailed soil map was obtained from Bazaglia Filho et al. (2013). The SOCS and SOCS differences were compared with geology and pedology maps and their temporal changes were analyzed for each soil and geology type. Additionally, the SOCS and SOCS differences were also compared visually with a clay map for 0–20 cm and 80–100 cm layers obtained by Mendes et al. (2021b).

### 2.6. SOCS saturation and deficit estimation

For the region where the study area is located, Rodríguez-Albarracín et al. (2023) obtained a map of SOC saturation potential ($SOC_{Sat}$), which represents the amount of SOC that can be stored in the soil fine fraction through association with minerals. The difference between the SOCS associated with minerals ($SOCS_{Moan}$) in 1997 and 2022 and the $SOCS_{Sat}$ represents the SOCS deficit ($SOCS_{Def}$) for each period, i.e., the amount that soil fine fraction can still sequester (Rodríguez-Albarracín et al., 2023). To evaluate the $SOCS_{Def}$ for each period and depth, these analyses were performed for the 0–20 cm and 80–100 cm using the best maps obtained from the best strategy. The results were also stratified by soil class.

First, the $SOC_{Sat}$ map from Rodríguez-Albarracín et al. (2023) for the 0–20 cm and 80–100 cm layers were converted to $SOCS_{Sat}$. We used the equation $SOCS_{Sat}$ (ton $ha^{-1}$) = $SOC_{Sat}$ (g $kg^{-1}$) x BD (g $cm^{-3}$) x t (cm) / 10, where t = 20 cm. The BD was obtained using the Benites et al. (2007) pedotransfer function: BD (g $cm^{-3}$) = 1.5688 – (0.0005 x Clay (g $kg^{-1}$)) – (0.0090 x $SOC_{Sat}$ (g $kg^{-1}$)), and the clay maps were obtained from Mendes et al. (2021b). The SOCS maps for 1997 and 2022 for both layers were converted to $SOCS_{Moan}$ using the equation developed by Rodríguez-Albarracín et al. (2023): $SOCS_{Moan}$ = 0.8966 x SOCS + 0.0773. Finally, the $SOCS_{Def}$ for each period and layers were calculated as follows: $SOCS_{Def}$ = $SOCS_{Moan}$ - $SOCS_{Sat}$.

## 3. Results

### 3.1. SOCS descriptive analyses

There was an increase of SOCS content from 1997 to 2022 (Fig. 2). Considering the training dataset, the SOCS increased from 27.15 ton $ha^{-1}$ with standard deviation (sd) of 13.83 ton $ha^{-1}$ in 1997–30.51 ton $ha^{-1}$ with an sd of 9.94 ton $ha^{-1}$ in 2022 for the 0–20 cm layer. Similarly, for 80–100 cm depth, an increase was observed from 9.74 ton $ha^{-1}$ with an sd of 7.67 ton $ha^{-1}$ in 1997–16.41 ton $ha^{-1}$ with an sd of 5.64 ton $ha^{-1}$ in 2022. The test dataset for 1997 showed a mean value of 25.26 ton $ha^{-1}$ with an sd of 12.28 ton $ha^{-1}$ for the 0–20 cm layer and a mean value of 6.40 ton $ha^{-1}$ with an sd of 5.09 ton $ha^{-1}$ for the 80–100 cm layer.

### 3.2. SOCS predicted maps

For strategy 1, two Cubist models were built (Fig. 3ab). The first model, called Model 1, was built with the 1997 dataset, achieving $R^2$ of 0.54, RMSE of 10.25 ton $ha^{-1}$, and RPIQ of 1.91. The second model, called Model 2, was built with the 2022 dataset, achieving $R^2$ of 0.56, RMSE of 7.51 ton $ha^{-1}$, and RPIQ of 2.16. Each model was used to predict SOCS for the 0–20 cm and 80–100 cm layers of the respective periods. A visual inspection revealed an increase in SOCS from 1997 to 2022. For strategy 2, Model 2 was used to predict the maps for both periods and layers, and visually, few variations were observed from 1997 to 2022 (Fig. 3c). For strategy 3, Model 3 was built using data from both periods, achieving $R^2$ of 0.57, RMSE of 8.69 ton $ha^{-1}$, and RPIQ of 1.99 (Fig. 3d). A visual inspection revealed an increase in SOCS from 1997 to 2022, similar to that observed in strategy 1.

### 3.3. Environmental covariates importance

The dynamic and static covariates showed similar importance for SOCS modelling in Model 3, accounting for 52% and 48%, respectively (Fig. 4). Stratifying the results by SCORPAN factors, the “soil” factor, represented by soil attributes maps and used as static covariates, showed the highest importance (36.6%), with emphasis on soil chemical elements and mineralogy composition (Si, Al and Fe from XRF analyses and kaolinite relative amount from DRS). The SySi image bands, representing the soil, parent material, and time as dynamic covariates, showed an importance of 24%. The “organism” factor, represented by the Landsat

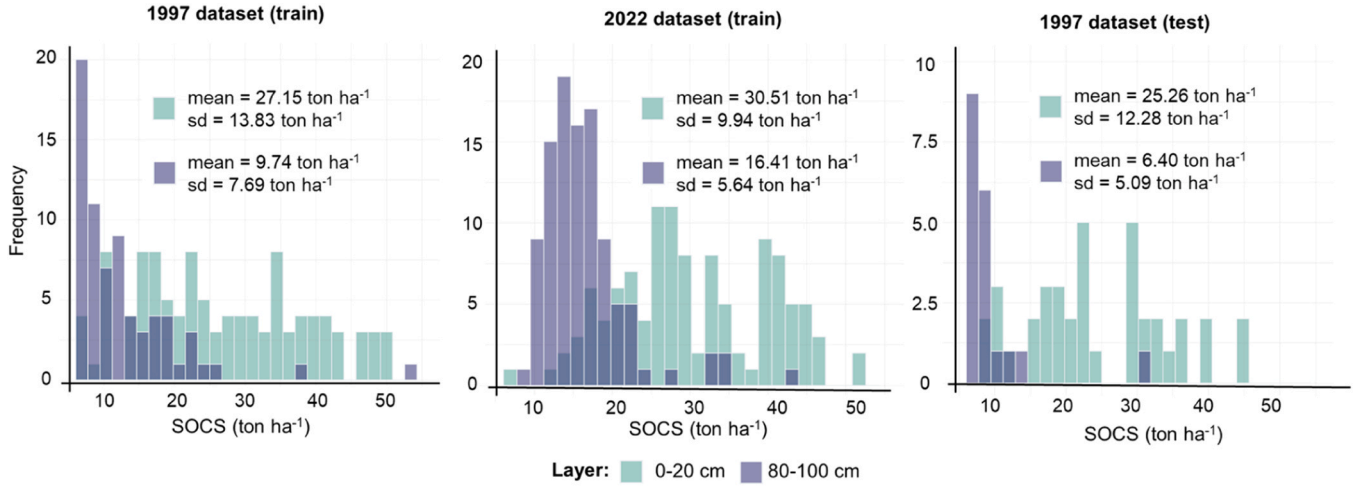


**Fig. 2.** Soil organic carbon stock (SOCS) descriptive statistics of calibration and validation datasets. sd = standard deviation.

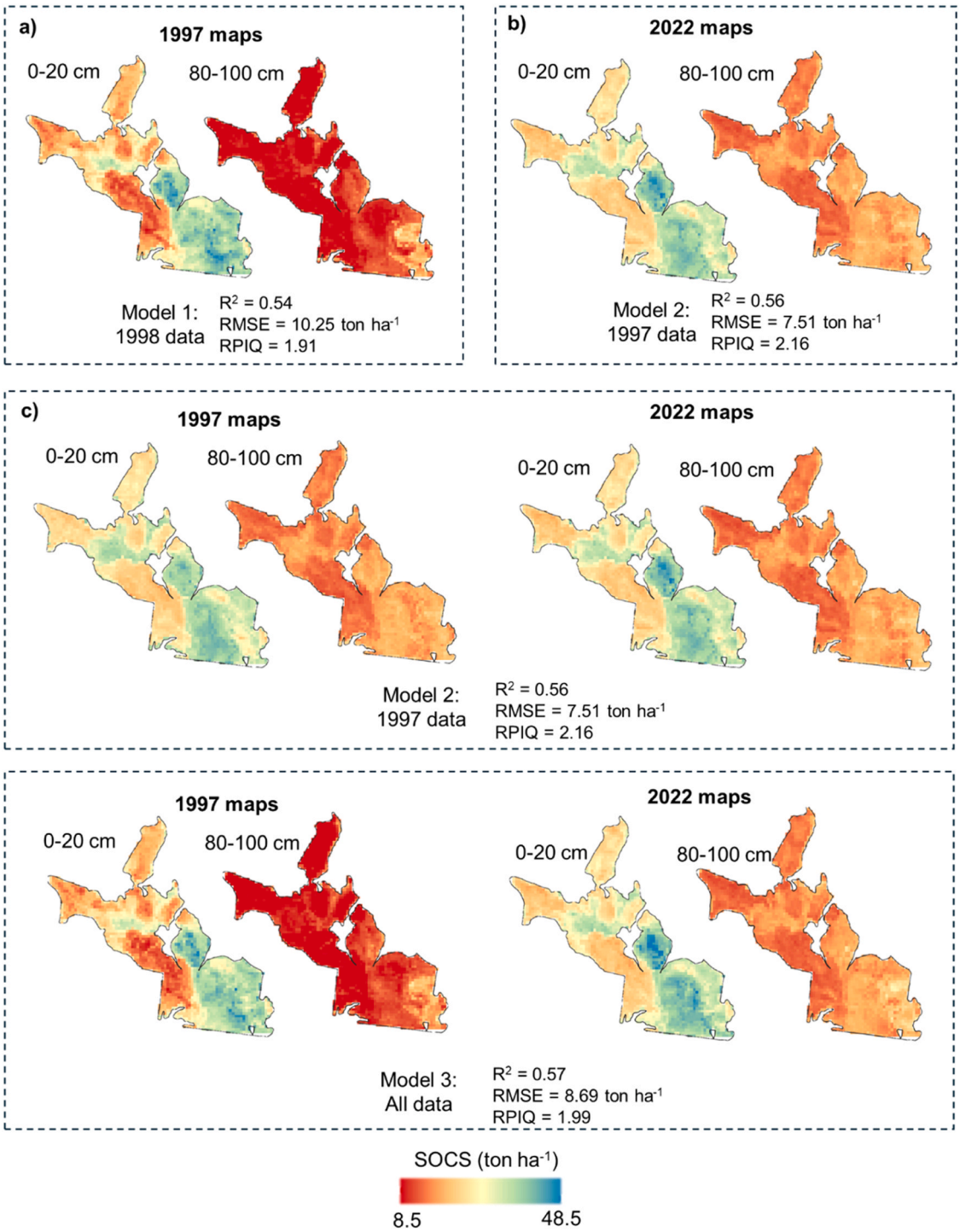


**Fig. 3.** Modelling accuracy and predicted soil organic carbon stock (SOCS) maps using strategy 1 (a), 2 (b) and 3 (c). $R^2$ = coefficient of determination; RMSE = root mean square error; RPIQ = ratio of interquartile internal.

bands and the NDVI index derived from these bands and used as dynamic covariates, showed an importance of 20.4%. The other covariates representing relief, time, climate, and soil together accounted for 19.1% of the importance. The rules of the Cubist Model 3 are provided in Supplementary material.

### 3.4. External validation

In external validation, strategy 2 resulted in more biased predictions for the 1997 period and showed higher SOCS predicted values than strategies 1 and 3 (Fig. 5). The most accurate results were observed for strategy 3. For strategy 1, the external validation achieved $R^2$ of 0.74, RMSE of 7.69 ton $ha^{-1}$ and a Bias of 3.43 ton $ha^{-1}$ in (Fig. 5a). In this strategy, the predicted map for 0–20 cm layer showed a mean value of 27.73 ton $ha^{-1}$ with an sd of 10.31 ton $ha^{-1}$, while the 80–100 cm layer map showed a mean value of 10.40 ton $ha^{-1}$, with an sd of 3.83 ton $ha^{-1}$. For strategy 2, we observed $R^2$ of 0.71, RMSE of 11.06 ton $ha^{-1}$, and Bias of 7.93 ton $ha^{-1}$ (Fig. 5b). In this strategy, the predicted map for the 0–20 cm layer showed a mean value of 30.12 ton $ha^{-1}$, with an sd of 6.44 ton $ha^{-1}$, while the 80–100 cm layer map showed mean value of

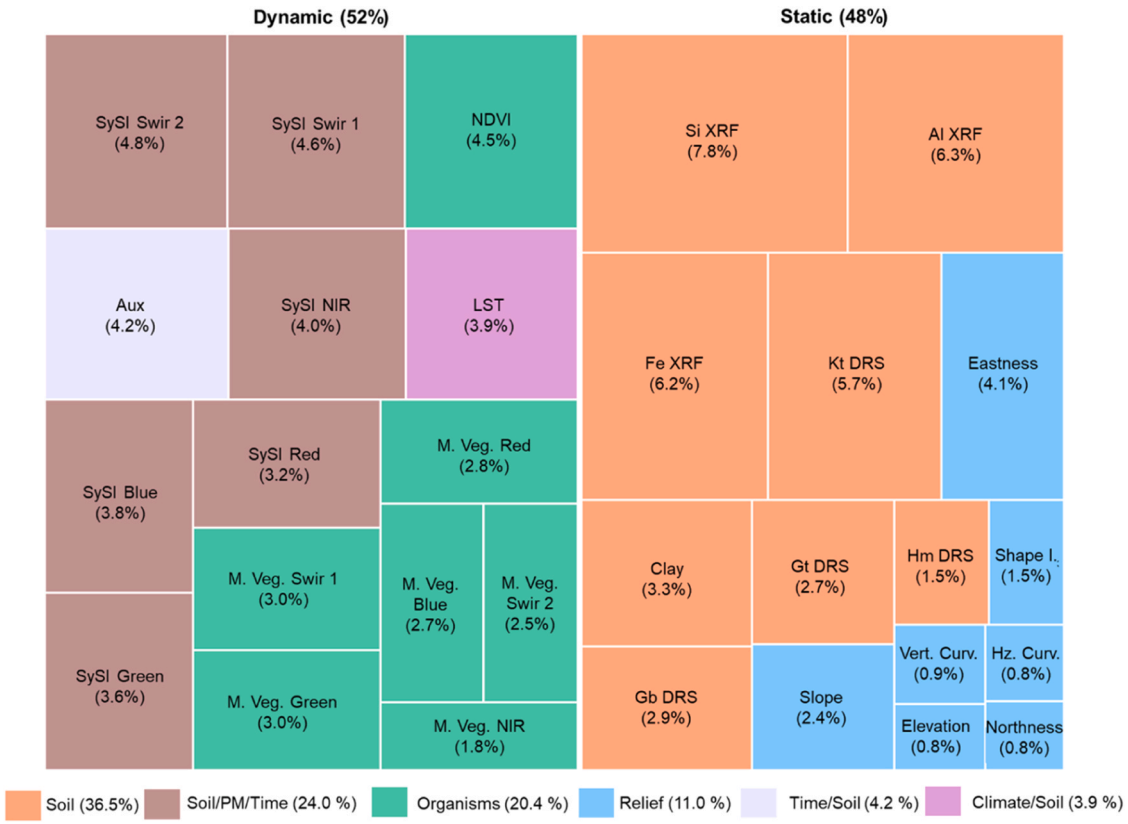


**Fig. 4.** Static and dynamic environmental covariates importance. SySi= bare soil image; Swir= short wave infrared; NIR = near infrared; NDVI = normalized difference vegetation index; Aux= Auxiliar; LST = land surface temperature; M. Veg. = Mosaic of vegetation; XRF= X-ray fluorescence; DRS = diffuse reflectance spectroscopy; Kt = kaolinite; Gt = goethite; Hm = hematite; Gb = gibbsite; Shape I. = shape index; Vert. Curv. = vertical curvature; Hz. Curv = horizontal curvature; PM = parent material.

17.09 ton ha$^{-1}$, with an sd of 2.35 ton ha$^{-1}$. For strategy 3, we observed $R^2$ of 0.76, RMSE of 7.19 ton ha$^{-1}$, and Bias of 3.25 ton ha$^{-1}$ (Fig. 5c). In this strategy, the predicted map for the 0–20 cm layer showed a mean value of 27.35 ton ha$^{-1}$ with an sd of 10.11 ton ha$^{-1}$, while the 80–100 cm layer map showed a mean value of 10.44 ton ha$^{-1}$, with an sd of 3.43 ton ha$^{-1}$.

### 3.5. SOCS temporal dynamic and deficit

From 1997–2022, SOCS increased in almost all regions of the area in both layers, with a more pronounced increase in the 80–100 cm layer (Fig. 6a). The SOCS increased by 3.54 ton ha$^{-1}$ for the 0–20 cm and by 6.09 ton ha$^{-1}$ for 80–100 cm layer (Fig7ab). There was a reduction in BSF in almost all areas from the 1997–1998 period to 2021–2022 period (Fig. 6b) and from the 1990–2002 period to 2010–2022 period (Fig. 6c). Significant negative correlations were found between SOCS and BSF, ranging from −0.15 to −0.50 for the 0–20 cm layer and from −0.25 to −0.47 for 80–100 cm layer.

All soil classes showed SOCS increase from 1997 to 2022 in both layers (Fig. 6d and 7ab). The greatest increase for the 0–20 cm layer was observed in Yellow Lixisols (8.27 ton ha$^{-1}$), followed by Red Yellow Lixisols (5.39 ton ha$^{-1}$), Nitisols (4.43 ton ha$^{-1}$), Gleysols (3.94 ton ha$^{-1}$), Cambisols (3.62 ton ha$^{-1}$) and Red Nitisols (2.47 ton ha$^{-1}$). Chernozens (0.94 ton ha$^{-1}$) and Leptosols (0.01 ton ha$^{-1}$) showed the lowest mean increases, with a decrease in some parts of the study area. For the 80–100 cm layer, the greatest increase was observed in Nitisols (7.88 ton ha$^{-1}$), followed by Red Yellow Lixisols (6.65 ton ha$^{-1}$), Cambisols (6.31 ton ha$^{-1}$), Gleysols (5.90 ton ha$^{-1}$), Red Nitisols (5.86 ton ha$^{-1}$), Yellow Lixisols (5.38 ton ha$^{-1}$), Chernozens (4.82 ton ha$^{-1}$) and Leptosols (3.87 ton ha$^{-1}$).

All geology types also showed an increase from 1997 to 2022 for both layers (Fig. 6e and 7 cd). The greatest increase for the 0–20 cm layer was observed in Siltstones (5.29 ton ha$^{-1}$), followed by Alluvial deposits (3.83 ton ha$^{-1}$), Metamorphosed Siltstones (3.56 ton ha$^{-1}$), and Diabases (2.12 ton ha$^{-1}$). For the 80–100 cm layer, the greatest increase was also observed in Siltstones (6.63 ton ha$^{-1}$), followed by Alluvial deposits (6.51 ton ha$^{-1}$), Metamorphosed Siltstones (6.43 ton ha$^{-1}$), and Diabases (5.49 ton ha$^{-1}$).

The area had a SOCS saturation potential up to 47 ton ha$^{-1}$, mainly related to clayey soils and in 80–100 cm depth (Fig 8ab). The SOCS deficit decreased from 1997 to 2022 due to the fixation of new carbon (C) in the soil in both layers (Fig. 8cb). Most of the study area is below the saturation potential in both periods, whit a small proportion of the area having more SOC than the saturation potential, mainly in 2022 period.

## 4. Discussion

The sampled grid at the exact same locations showed that the area exhibited a generalized increase in SOCS from 1997 to 2022 (Fig. 2). The land use in the study area remained unaltered between the two periods, with sugarcane cultivation throughout. Thus, the likely explanation for SOCS increase is the drastic change in sugarcane management that occurred in the 2000s in the region where the study area is located, when the conventional system with the pre-harvesting burning was replaced by mechanized harvesting without burning (green harvesting) (Aguiar et al., 2011; Campos et al., 2022). São Paulo State law nº 11.241 of 2002 established a deadline for the end of burning, and pre-harvest burning areas have reached levels close to zero in the state nowadays (Campos et al., 2022). Furthermore, the adoption of good management

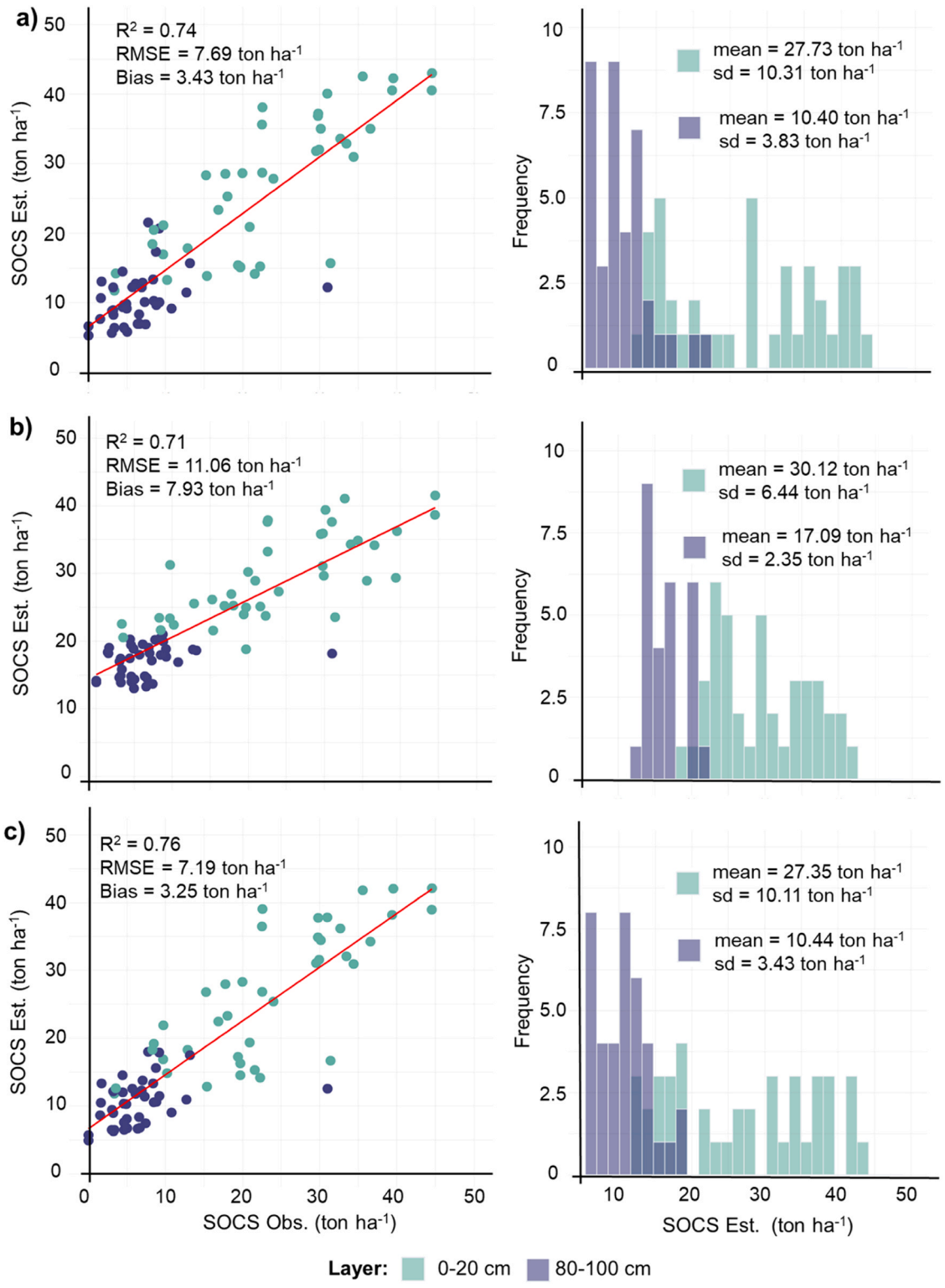


**Fig. 5.** External validation for 1997 using the strategies 1(a), 2 (b) e 3 (c). $R^2$ = coefficient of determination; RMSE = root mean square error; sd = standard deviation; SOCS = Soil organic carbon stock; Obs.= observed; Est. = estimated.

practices, such as conservative tillage, crop residues management, by-product recycling, and rational fertilization, may have contributed to the SOCS increase (Cherubin et al., 2021).

Strategy 1 is similar to non-temporal DSM, where two independent models were used to predict each period without temporal extrapolation. It resulted in reliable maps, representing the variation observed in the sampled points (Fig. 2 and Fig. 3ab), while the external validation indicated accurate and unbiased results (Fig. 4a). A limitation of this approach is that sufficient soil data are needed in each period to calibrate at least two independent models, preferably from points at the exact same locations. We found results similar to those of Nguemezi et al. (2021), who mapped SOCS at a regional scale in 1985 and 2017, achieving $R^2$ of 0.62 and RMSE of 11.61 ton $ha^{-1}$ in the first period and $R^2$ of 0.58 and RMSE of 13.15 ton $ha^{-1}$ in the second period using

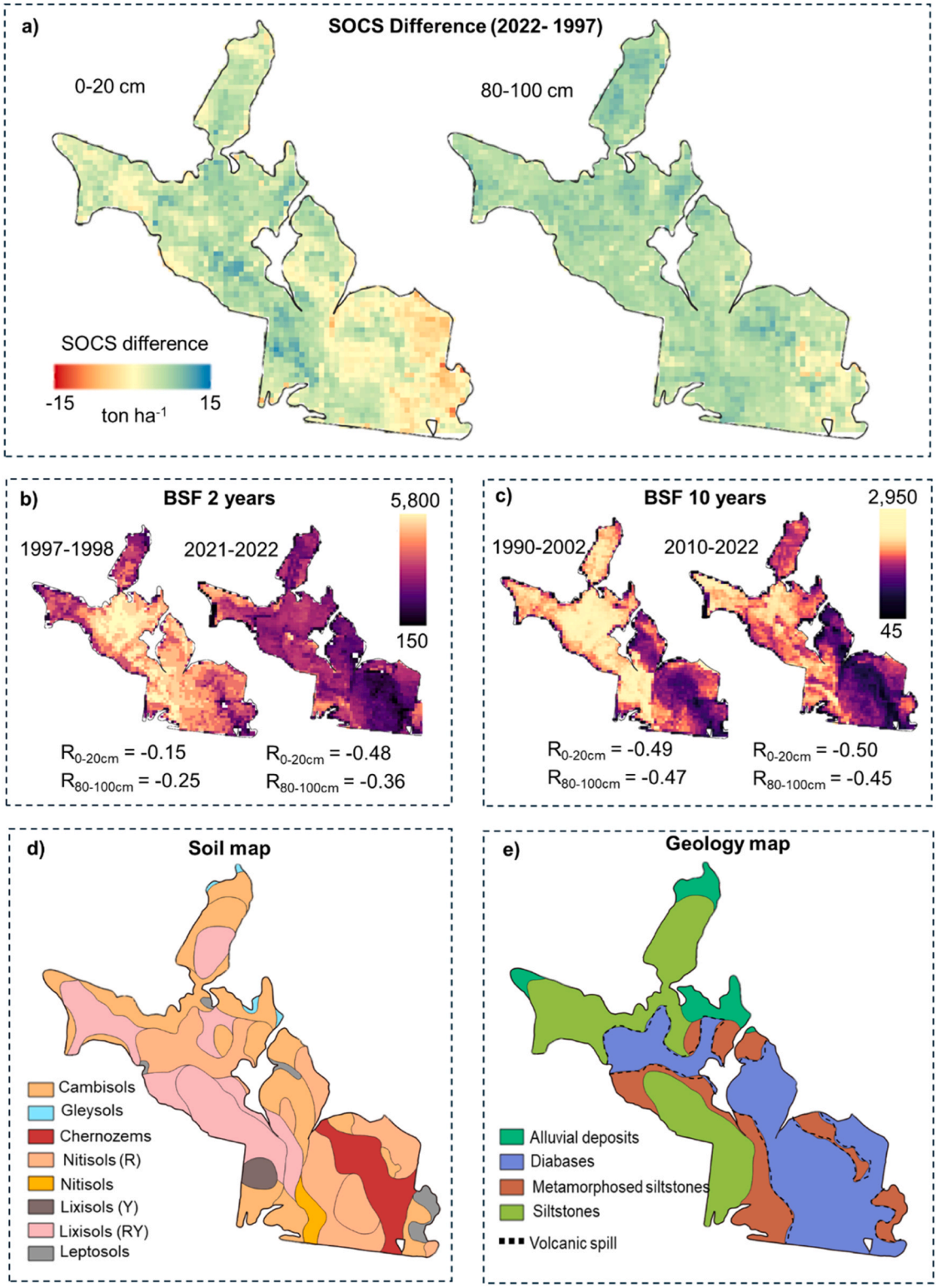


**Fig. 6.** Soil organic carbon stock (SOCS) difference between 1997 and 2022 (a), bare soil frequency (BSF) for 2 (b) and 10 (c) year periods, and soil (d) and geology (e) maps. R= red; Y = yellow; RY = red-yellow.

10-fold CV. Similarly, Bartsch et al. (2025) used similar approach for SOC content mapping in an agricultural area (pasture and soybean) considering 2013/2014 and 2020/2021 periods, achieving $R^2$ of 0.47, RMSE of 3.11 g $kg^{-1}$, and RPIQ of 0.63 for the first period and $R^2$ of 0.25, RMSE of 3.08 g $kg^{-1}$, and RPIQ of 0.74 for the second period in the validation dataset (30% of data) for each period, respectively. Szatmári et al. (2019) evaluated the SOC stock changes from 1992 to 2010 across all Hungary and found an RMSE of 21.99 and 21.39 ton $ha^{-1}$ in 10-fold CV for the first and second periods, respectively.

Strategy 2 presented more biased results, with the predicted map for 1997 not reflecting the SOCS observed in the sampling points (Fig. 2, Fig. 3c and Fig. 4b). The predicted values were higher than the observed

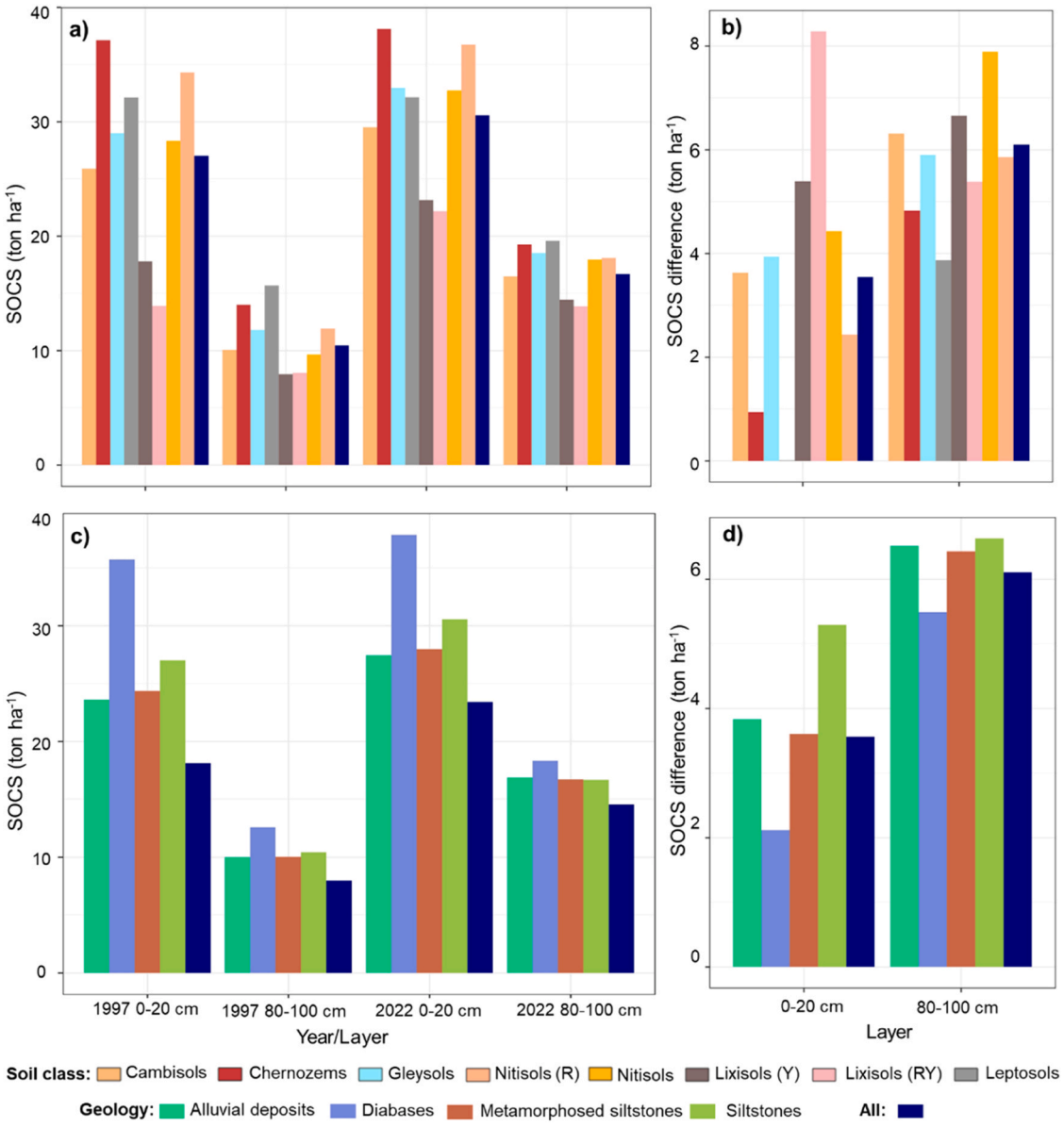


**Fig. 7.** Soil organic carbon stock (SOCS) (a) and SOCS difference (b) by soil classes, and SOCS (c) and SOCS difference (d) by geology.

values, indicating that the 2022 model (Model 2) did not perform reliable predictions for a different period without samples in the training dataset (Fig. 4b). Strategy 2 is used in literature mainly to make future predictions, where a model calibrated in the present or past can be used to predict the SOC in the future under climate change scenarios (Chen et al., 2024; Wang et al., 2022; Yigini and Panagos, 2016). On the other hand, Bartsch et al. (2025) successfully used a multitemporal model with data from two periods (2013/2014 and 2020/2021) to predict the SOC content for intermediate periods (2014/2015, 2016/2017 and 2018/2019). However, it is important to point out that the range of all SOC data from these intermediate periods was covered by the multitemporal model of Bartsch et al. (2025), differing from the present study, in which a dataset from a period of higher SOCS was used to predict a period with lower SOCS, this is exactly what occur in the studies of future predictions.

The best results were observed for strategy 3, comprising a multitemporal model with points for both periods (Model 3) (Fig. 2, Fig. 3d and Fig. 4c). Besides slightly better statistical parameters in external validation, this strategy had other advantages compared to strategy 1. Strategy 3 requires relatively few available points for model training and can be performed with an irregular number of points across different time periods. Bartsch et al. (2025) (described above) used a multitemporal model for SOC content predictions at the farm scale, achieving $R^2$ of 0.34, RMSE of 3.11 g $kg^{-1}$, and RPIQ of 0.76 in the validation dataset (30% of data) for each period. Heuvelink et al. (2021) mapped SOCS for the whole of Argentina across several periods from 1982 to 2017 using a single model, with an RMSE of 20.4 ton $ha^{-1}$ in 10-fold CV. Ugbaje et al. (2024) did the same from 1990 to 2018 across Australia, with an RMSE of 31.43 ton $ha^{-1}$.

The soil attributes map as a whole, static covariates representing the soil chemical constitution, mineralogy and texture, showed the highest importance in the modelling (Fig. 3). These attributes are closely related to SOC fixation, retention, and dynamics. The soil chemical composition, which is still little explored in spatial analyses, showed a strong relation to SOC (Rosin et al., 2024, 2022), with Si, Al, and Fe showing the highest importance individually. The six SySY bands also showed great importance, since they provide a direct measurement of soil reflectance, representing the "soil" factor directly and the "parent material" and "time" factors indirectly (Mendes et al., 2021b; Poppiel et al., 2020). The vegetation reflectance and NDVI index also achieved great

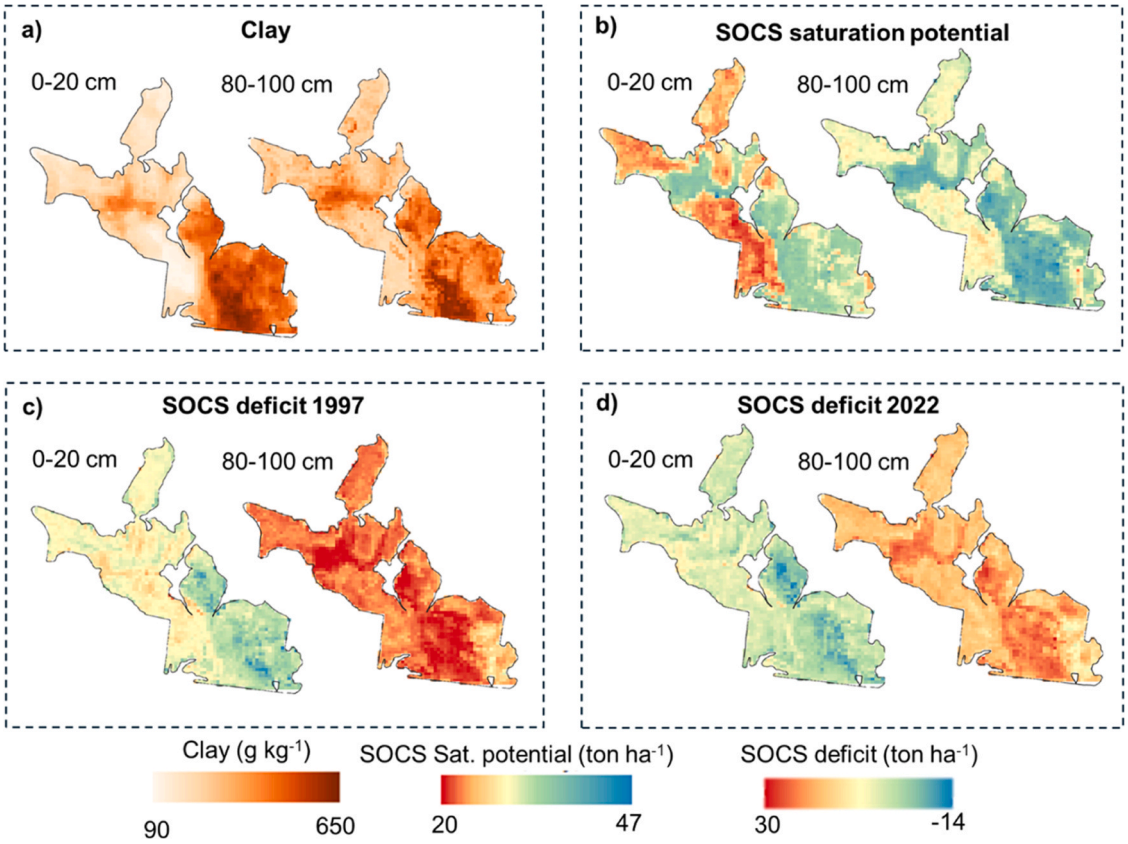


**Fig. 8.** Clay content (a), soil organic carbon stock (SOCS) saturation potential (b) and SOCS deficit for 1997 (c) and 2022 (d) years.

importance, since the vigor of vegetation is indirectly related to SOCS, and is widely used as dynamic covariate for its temporal mapping (Bartsch et al., 2025; Heuvelink et al., 2021; Ugbaje et al., 2024).

The BSF represents how many times a given pixel was exposed in a satellite image time series (Demattê et al., 2020). We verified a decrease in BSF from 1997 to 2022, which can be associated with SOCS increase (Fig. 6abc). Sousa et al. (2024) and Campos et al. (2022) also reported a decrease in BSF and associated it with the end of pre-harvest burning in São Paulo State and specifically in the region of our study area, respectively. Lower BSF values can be associated with higher SOC values and with better soil conditions in general, since soil exposure is a driver of soil degradation, for example through erosion and SOC decomposition (Demattê et al., 2020; Sousa et al., 2024).

The SOCS increased for all soil and geology types, with the soil classes Leptosols and Chrenozens showing smaller increases and even decreases in some locations (Figs. 6 and 7). The SOCS increased from 1997 to 2022, likely due to changes in sugarcane management mentioned above. Chernozems and Leptosol are less weathered, contain lower iron oxide contents, have less aggregation, and have naturally high SOC content compared to the other soils classes in the study area (Buol et al., 2011; IUSS Working Group WRB, 2015), which may contribute to the smaller increases and the decreases at some specific points. Furthermore, areas with high native SOCS showed decreases in a national SOCS dynamic study, particularly under sugarcane cultivation (Rosin et al., 2026).

Rodríguez-Albarracín et al. (2023) mapped the $SOCS_{Sat}$, which represents the potential of SOC fixation associated with minerals in the clay fraction (Fig. 8ab). In general, the 80–100 cm layer has a greater potential to sequester new carbon (C) because of its higher clay content. Similarly, the SOCS deficit was greater in the 80–100 cm layer because the current SOCS is lower at this depth (Fig. 8 cd). The SOCS deficit decreased from 1997 to 2022, particularly in the 80–100 cm layer, due to the increase of SOCS in the area. The subsoil of agricultural areas has great potential to sequester SOC and mitigate climate change (Button et al., 2022). This approach comparing the 1997 and 2022 deficit highlighted the importance of spatial-temporal SOCS mapping for accessing the current soil condition, for evaluating agricultural management practices and policies related to C sequestration, and for accessing the possibility of sequestering new C from the atmosphere.

## 5. Conclusions

The SOCS showed a considerable increase from 1997 to 2022, probably due to changes in sugarcane management, such as the end of pre-harvest burning. Strategies 1 (an independent model for each period) and 3 (a multitemporal model) produced accurate and less biased maps, while strategy 2 (extrapolation from one period to another without points) was not efficient. Strategy 3 is particularly useful for SOCS mapping when limited temporal observations are available. Soil attributes, mainly total chemical elements from XRF, were most important covariates for modeling, followed by the bare soil image (SySI) and vegetation information. The bare soil frequency (BSF), an important proxy for soil condition monitoring, showed an inverse relation with SOCS. Soil type and geology also influenced SOC dynamic. Finally, it is possible to evaluate the SOCS saturation deficit by spatio-temporal mapping.

## CRediT authorship contribution statement

**Jean Jesus Macedo Novais:** Writing – review & editing. **Bruno dos Anjos Bartsch:** Writing – review & editing. **Jorge Tadeu Fim Rosas:** Writing – review & editing. **Heidy Soledad Rodríguez-Albarracín:** Writing – review & editing, Writing – original draft. **José A.M. Demattê:** Writing – review & editing, Visualization, Supervision, Project administration, Funding acquisition, Conceptualization. **Nícolas Augusto Rosin:** Writing – review & editing, Writing – original draft,

Visualization, Validation, Software, Methodology, Funding acquisition, Formal analysis, Conceptualization. **Renan Falcioni:** Writing – review & editing. **Danilo César de Mello:** Writing – review & editing. **Carlos Eduardo Pellegrino Cerri:** Writing – review & editing. **Marcelo Henrique Procópio Pelegrino:** Writing – review & editing.

## Funding

This work was supported by São Paulo Research Foundation (FAPESP) [Grant Numbers: 2014/22262–0, 2021/10063–6, 2021/05129–8, 2021-10573-4 and 2024/06285-1] and by National Council for Scientific and Technological Development - Brazil (CNPq) [Grant Numbers: 307190-2021-8 and 402895/2025-8]. The Article Processing Charge for the publication of this research was funded by the Coordenação de Aperfeiçoamento de Pessoal de Nível Superior - Brasil (CAPES).

## Declaration of Competing Interest

The authors declare that they have no known competing financial interests or personal relationships that could have appeared to influence the work reported in this paper.

## Acknowledgments

The authors also thank the Department of Soil Science of Esalq/USP and the members of the Geotechnologies in Soil Science Group (GeoCIS/GeoSS) (https://esalqgeocis.wixsite.com/english)

## Appendix A. Supporting information

Supplementary data associated with this article can be found in the online version at doi:10.1016/j.still.2026.107354.

## Data Availability

Data will be made available on request.

## References

Adhikari, K., Hartemink, A.E., Minasny, B., Bou Kheir, R., Greve, M.B., Greve, M.H., 2014. Digital Mapping of Soil Organic Carbon Contents and Stocks in Denmark. PLoS. One 9, e105519. https://doi.org/10.1371/journal.pone.0105519.

Aguiar, D.A., Rudorff, B.F.T., Silva, W.F., Adami, M., Mello, M.P., 2011. Remote Sensing Images in Support of Environmental Protocol: Monitoring the Sugarcane Harvest in São Paulo State, Brazil. Remote. Sens. (Basel) 3, 2682–2703. https://doi.org/10.3390/rs3122682.

Alvares, C.A., Stape, J.L., Sentelhas, P.C., de Moraes Gonçalves, J.L., Sparovek, G., 2013. Köppen's climate classification map for Brazil. Meteorol. Z. 22, 711–728. https://doi.org/10.1127/0941-2948/2013/0507.

Bartsch, B. dos A., Rosin, N.A., Rosas, J.T.F., Poppiel, R.R., Makino, F.Y., Vogel, L.G., Novais, J.J.M., Falcioni, R., Alves, M.R., Demattê, J.A.M., 2025. Space-time mapping of soil organic carbon through remote sensing and machine learning. Soil. Tillage Res. 248, 106428. https://doi.org/10.1016/j.still.2024.106428.

Bazaglia Filho, O., Rizzo, R., Lepsch, I.F., Prado, H. do, Gomes, F.H., Mazza, J.A., Demattê, J.A.M., 2013. Comparison between detailed digital and conventional soil maps of an area with complex geology. Rev. Bras. Cienc. Solo 37, 1136–1148. https://doi.org/10.1590/S0100-06832013000500003.

Benites, V.M., Machado, P.L.O.A., Fidalgo, E.C.C., Coelho, M.R., Madari, B.E., 2007. Pedotransfer functions for estimating soil bulk density from existing soil survey reports in Brazil. Geoderma 139, 90–97. https://doi.org/10.1016/j.geoderma.2007.01.005.

Bouyoucos, G.J., 1962. Hydrometer Method Improved for Making Particle Size Analyses of Soils 1. Agron. J. 54, 464–465. https://doi.org/10.2134/agronj1962.00021962005400050028x.

Buol, S.W., Southard, R.J., Graham, R.C., McDaniel, P.A., 2011. Soil Genesis and Classification. 6a, ed. ,. John Wiley & Sons Ltd, Chichester, UK.

Button, E.S., Pett-Ridge, J., Murphy, D.V., Kuzyakov, Y., Chadwick, D.R., Jones, D.L., 2022. Deep-C storage: Biological, chemical and physical strategies to enhance carbon stocks in agricultural subsoils. Soil. Biol. Biochem. 170, 108697. https://doi.org/10.1016/j.soilbio.2022.108697.

Campos, L.R., Demattê, J.A.M., Bellinaso, H., Poppiel, R.R., Greschuk, L.T., Rizzo, R., Rosin, N.A., Rosas, J.T.F., 2022. Detection of bare soils in sugarcane areas by temporal satellite images: A monitoring technique for soil security. Soil. Secur. 7, 100057. https://doi.org/10.1016/j.soisec.2022.100057.

Castaldi, F., Halil Koparan, M., Wetterlind, J., Žydelis, R., Vinci, I., Özge Savaş, A., Kıvrak, C., Tunçay, T., Volungevičius, J., Obber, S., Ragazzi, F., Malo, D., Vaudour, E., 2023. Assessing the capability of Sentinel-2 time-series to estimate soil organic carbon and clay content at local scale in croplands. ISPRS J. Photogramm. Remote. Sens. 199, 40–60. https://doi.org/10.1016/j.isprsjprs.2023.03.016.

Chen, B., Lu, Q., Wei, L., Fu, W., Wei, Z., Tian, S., 2024. Global predictions of topsoil organic carbon stocks under changing climate in the 21st century. Sci. Total. Environ. 908, 168448. https://doi.org/10.1016/j.scitotenv.2023.168448.

Cherubin, M.R., Carvalho, J.L.N., Cerri, C.E.P., Nogueira, L.A.H., Souza, G.M., Cantarella, H., 2021. Land Use and Management Effects on Sustainable Sugarcane-Derived Bioenergy. Land 10, 72. https://doi.org/10.3390/land10010072.

R. Core Team, 2024. R: A language and environment for statistical computing [WWW Document]. URL ⟨https://www.R-project.org/⟩ (accessed 6.17.24).

Demattê, J.A.M., Fongaro, C.T., Rizzo, R., Safanelli, J.L., 2018. Geospatial Soil Sensing System (GEOS3): A powerful data mining procedure to retrieve soil spectral reflectance from satellite images. Remote. Sens. Environ. 212, 161–175. https://doi.org/10.1016/j.rse.2018.04.047.

Demattê, J.A.M., Safanelli, J.L., Poppiel, R.R., Rizzo, R., Silvero, N.E.Q., Mendes, W., de, S., Bonfatti, B.R., Dotto, A.C., Salazar, D.F.U., Mello, F.A., de, O., Paiva, A.F., da, S., Souza, A.B., Santos, N.V., dos, Maria Nascimento, C., Mello, D.C., de, Bellinaso, H., Gonzaga Neto, L., Amorim, M.T.A., Resende, M.E.B., de, Vieira, J., da, S., Queiroz, L.G., de, Gallo, B.C., Sayão, V.M., Lisboa, C.J., da, S., 2020. Bare Earth's Surface Spectra as a Proxy for Soil Resource Monitoring. Sci. Rep. 10, 1–11. https://doi.org/10.1038/s41598-020-61408-1.

Ermida, S.L., Soares, P., Mantas, V., Göttsche, F.-M., Trigo, I.F., 2020. Google Earth Engine Open-Source Code for Land Surface Temperature Estimation from the Landsat Series. Remote. Sens. 12, 1471. https://doi.org/10.3390/rs12091471.

Evangelista, S.J., Field, D.J., McBratney, A.B., Minasny, B., Ng, W., Padarian, J., Román Dobarco, M., Wadoux, A.M.J.-C., 2024. Soil. Secur. Strateg. a Sustain. Future Soil. 1–70. https://doi.org/10.1016/bs.agron.2023.10.001.

Farr, T.G., Kobrick, M., 2000. Shuttle radar topography mission produces a wealth of data. Eos Trans. Am. Geophys. Union. 81, 583. https://doi.org/10.1029/EO081i048p00583.

Feeney, C.J., Bentley, L., De Rosa, D., Panagos, P., Emmett, B.A., Thomas, A., Robinson, D.A., 2024. Benchmarking soil organic carbon (SOC) concentration provides more robust soil health assessment than the SOC/clay ratio at European scale. Sci. Total. Environ. 951, 175642. https://doi.org/10.1016/j.scitotenv.2024.175642.

Gomes, L.C., Faria, R.M., de Souza, E., Veloso, G.V., Schaefer, C.E.G.R., Filho, E.I.F., 2019. Modelling and mapping soil organic carbon stocks in Brazil. Geoderma 340, 337–350. https://doi.org/10.1016/j.geoderma.2019.01.007.

Gorelick, N., Hancher, M., Dixon, M., Ilyushchenko, S., Thau, D., Moore, R., 2017. Google Earth Engine: Planetary-scale geospatial analysis for everyone. Remote. Sens. Environ. 202, 18–27. https://doi.org/10.1016/j.rse.2017.06.031.

Hengl, T., Mendes de Jesus, J., Heuvelink, G.B.M., Ruiperez Gonzalez, M., Kilibarda, M., Blagotić, A., Shangguan, W., Wright, M.N., Geng, X., Bauer-Marschallinger, B., Guevara, M.A., Vargas, R., MacMillan, R.A., Batjes, N.H., Leenaars, J.G.B., Ribeiro, E., Wheeler, I., Mantel, S., Kempen, B., 2017. SoilGrids250m: Global gridded soil information based on machine learning. PLoS. One 12, e0169748. https://doi.org/10.1371/journal.pone.0169748.

Heuvelink, G.B.M., Angelini, M.E., Poggio, L., Bai, Z., Batjes, N.H., Bosch, R., Bossio, D., Estella, S., Lehmann, J., Olmedo, G.F., Sanderman, J., 2021. Machine learning in space and time for modelling soil organic carbon change. Eur. J. Soil. Sci. 72, 1607–1623. https://doi.org/10.1111/ejss.12998.

Hoffland, E., Kuyper, T.W., Comans, R.N.J., Creamer, R.E., 2020. Eco-functionality of organic matter in soils. Plant. Soil. 455, 1–22. https://doi.org/10.1007/s11104-020-04651-9.

IUSS Working Group WRB, 2015. World Reference Base for Soil Resources 2014. In: Update 2015. World Soil Resources Reports, 106. FAO, Rome.

Kempen, B., Dalsgaard, S., Kaaya, A.K., Chamuya, N., Ruipérez-González, M., Pekkarinen, A., Walsh, M.G., 2019. Mapping topsoil organic carbon concentrations and stocks for Tanzania. Geoderma 337, 164–180. https://doi.org/10.1016/j.geoderma.2018.09.011.

Kuhn, M., Wing, J., Weston, S., Williams, A., Keefer, C., Engelhardt, A., Kenkel, B., 2021. caret: Classification and Regression Training: R package version 6 [WWW Document]. URL (accessed 6.15.21).

Lal, R., 2016. Beyond COP 21: Potential and challenges of the "4 per Thousand" initiative. J. Soil. Water Conserv. 71, 20A–25A. https://doi.org/10.2489/jswc.71.1.20A.

Liptzin, D., Norris, C.E., Cappellazzi, S.B., Bean, G.Mac, Cope, M., Greub, K.L.H., Rieke, E.L., Tracy, P.W., Aberle, E., Ashworth, A., Bañuelos Tavarez, O., Bary, A.I., Baumhardt, R.L., Borbón Gracia, A., Brainard, D.C., Brennan, J.R., Briones Reyes, D., Bruhjell, D., Carlyle, C.N., Crawford, J.J.W., Creech, C.F., Culman, S.W., Deen, B., Dell, C.J., Derner, J.D., Ducey, T.F., Duiker, S.W., Dyck, M.F., Ellert, B.H., Entz, M.H., Espinosa Solorio, A., Fonte, S.J., Fonteyne, S., Fortuna, A.-M., Foster, J.L., Fultz, L.M., Gamble, A.V., Geddes, C.M., Griffin-LaHue, D., Grove, J.H., Hamilton, S.K., Hao, X., Hayden, Z.D., Honsdorf, N., Howe, J.A., Ippolito, J.A., Johnson, G.A., Kautz, M.A., Kitchen, N.R., Kumar, S., Kurtz, K.S.M., Larney, F.J., Lewis, K.L., Liebman, M., Lopez Ramirez, A., Machado, S., Maharjan, B., Martinez Gamiño, M.A., May, W.E., McClaran, M.P., McDaniel, M.D., Millar, N., Mitchell, J.P., Moore, A.D., Moore, P.A., Mora Gutiérrez, M., Nelson, K.A., Omondi, E.C., Osborne, S.L., Osorio Alcalá, L., Owens, P., Pena-Yewtukhiw, E.M., Poffenbarger, H.J., Ponce Lira, B., Reeve, J.R., Reinbott, T.M., Reiter, M.S., Ritchey, E.L., Roozeboom, K.L., Rui, Y., Sadeghpour, A., Sainju, U.M., Sanford, G.R., Schillinger, W.F., Schindelbeck, R.R.,

Schipanski, M.E., Schlegel, A.J., Scow, K.M., Sherrod, L.A., Shober, A.L., Sidhu, S.S., Solís Moya, E., St Luce, M., Strock, J.S., Suyker, A.E., Sykes, V.R., Tao, H., Trujillo Campos, A., Van Eerd, L.L., van Es, H., Verhulst, N., Vyn, T.J., Wang, Y., Watts, D.B., Wright, D.L., Zhang, T., Morgan, C.L.S., Honeycutt, C.W., 2022. An evaluation of carbon indicators of soil health in long-term agricultural experiments. Soil. Biol. Biochem. 172, 108708. https://doi.org/10.1016/j.soilbio.2022.108708.

McBratney, A.B., Mendonça Santos, M.L., Minasny, B., 2003. On digital soil mapping. Geoderma 117, 3–52. https://doi.org/10.1016/S0016-7061(03)00223-4.

Mendes, W., de, S., Demattê, J.A.M., Bonfatti, B.R., Resende, M.E.B., Campos, L.R., Costa, A.C.S. da, 2021a. A novel framework to estimate soil mineralogy using soil spectroscopy. Appl. Geochem. 127. https://doi.org/10.1016/j.apgeochem.2021.104909.

Mendes, W., de, S., Demattê, J.A.M., Silvero, N.E.Q., Rabelo Campos, L., 2021b. Integration of multispectral and hyperspectral data to map magnetic susceptibility and soil attributes at depth: A novel framework. Geoderma 385, 114885. https://doi.org/10.1016/j.geoderma.2020.114885.

Minasny, B., Malone, B.P., McBratney, A.B., Angers, D.A., Arrouays, D., Chambers, A., Chaplot, V., Chen, Z.-S., Cheng, K., Das, B.S., Field, D.J., Gimona, A., Hedley, C.B., Hong, S.Y., Mandal, B., Marchant, B.P., Martin, M., McConkey, B.G., Mulder, V.L., O'Rourke, S., Richer-de-Forges, A.C., Odeh, I., Padarian, J., Paustian, K., Pan, G., Poggio, L., Savin, I., Stolbovoy, V., Stockmann, U., Sulaeman, Y., Tsui, C.-C., Vågen, T.-G., van Wesemael, B., Winowiecki, L., 2017. Soil carbon 4 per mille. Geoderma 292, 59–86. https://doi.org/10.1016/j.geoderma.2017.01.002.

Nanni, M.R., 2000. Dados radiométricos obtidos em laboratório e no nível orbital na caracterização e mapeamento de solos. USP, Piracicaba.

Nguemezi, C., Tematio, P., Silatsa, F.B.T., Yemefack, M., 2021. Spatial variation and temporal decline (1985–2017) of soil organic carbon stocks (SOCS) in relation to land use types in Tombel area, South-West Cameroon. Soil. Tillage Res. 213, 105114. https://doi.org/10.1016/j.still.2021.105114.

Padarian, J., Stockmann, U., Minasny, B., McBratney, A.B., 2022. Monitoring changes in global soil organic carbon stocks from space. Remote. Sens. Environ. 281, 113260. https://doi.org/10.1016/j.rse.2022.113260.

Poppiel, R.R., Lacerda, M.P.C., Rizzo, R., Safanelli, J.L., Bonfatti, B.R., Silvero, N.E.Q., Demattê, J.A.M., 2020. Soil Color and Mineralogy Mapping Using Proximal and Remote Sensing in Midwest Brazil. Remote. Sens. 12, 1197. https://doi.org/10.3390/rs12071197.

QGIS Development Team, 2024. QGIS Geographic Information System.

Quinlan, J.R., 1992. Learning with continuous classes. In: Adams, A., Sterling, L. (Eds.), Proceedings AI'92, 5th Australian Conference on Artificial Intelligence. World Scientific, Singapore, pp. 343–348. https://doi.org/10.1142/9789814536271.

Rodríguez-Albarracín, H.S., Demattê, J.A.M., Rosin, N.A., Contreras, A.E.D., Silvero, N.E.Q., Cerri, C.E.P., Mendes, W., de, S., Tayebi, M., 2023. Potential of soil minerals to sequester soil organic carbon. Geoderma 436, 116549. https://doi.org/10.1016/j.geoderma.2023.116549.

Rodríguez-Albarracín, H.S., Demattê, J.A.M., Rosin, N.A., Amorim, M.T.A., Contreras, A.E.D., Andreote, F.D., Rosas, J.T.F., 2024. Soil organic carbon sequestration potential explained by mineralogical and microbiological activity using spectral transfer functions. Sci. Total. Environ. 947, 174652. https://doi.org/10.1016/j.scitotenv.2024.174652.

Román Dobarco, M., Wadoux, A.M.J.-C., Malone, B., Minasny, B., McBratney, A.B., Searle, R., 2023. Mapping soil organic carbon fractions for Australia, their stocks, and uncertainty. Biogeosciences 20, 1559–1586. https://doi.org/10.5194/bg-20-1559-2023.

Rosas, J.T.F., Demattê, J.A.M., Rosin, N.A., Bartsch, B., dos, A., Poppiel, R.R., Rodriguez-Albarracin, H.S., Novais, J.J.M., Pavinato, P.S., Ma, Y., Mello, D.C., de, Francelino, M.R., Alves, M.R., 2024. Geotechnologies on the phosphorus stocks determination in tropical soils: General impacts on society. Sci. Total. Environ. 938, 173537. https://doi.org/10.1016/j.scitotenv.2024.173537.

Rosin, N.A., Demattê, J.A.M., Leite, M.C.A., de Carvalho, H.W.P., Costa, A.C., Greschuk, L.T., Curi, N., Silva, S.H.G., 2022. The fundamental of the effects of water, organic matter, and iron forms on the pXRF information in soil analyses. Catena (Amst. ) 210, 105868. https://doi.org/10.1016/j.catena.2021.105868.

Rosin, N.A., Demattê, J.A.M., de Carvalho, H.W.P., Rodriguez-Albarracín, H.S., Rosas, J.T.F., Novais, J.J., Dalmolin, R.S.D., Alves, M.R., Falcioni, R., Tziolas, N., Mallah, S., de Mello, D.C., Francelino, M.R., 2024. Spatializing soil elemental concentration as measured by X-ray fluorescence analysis using remote sensing data. Catena (Amst. ) 240, 107988. https://doi.org/10.1016/j.catena.2024.107988.

Rosin, N.A., Demattê, J.A.M., Minasny, B., Poppiel, R.R., Bartsch, B. dos A., Rosas, J.T.F., Rodríguez-Albarracín, H.S., Cherubin, M.R., Cerri, C.E.P., Vicente, L.E., 2026. Soil organic carbon stock changes over 40 years in Brazil: a country-scale assessment using soil science-informed machine learning. Catena (Amst. ) 270, 110155. https://doi.org/10.1016/j.catena.2026.110155.

Rouse, J.W., Haas, R.H., Schell, J.A., Deering, D.W., Freden, S.C., 1973. Monitoring vegetation systems in the Great Plains with ERTS. Proc. 3rd Earth Resour. Technol. Satell. -1 619 Symp. 309–317.

Roy, D.P., Zhang, H.K., Ju, J., Gomez-Dans, J.L., Lewis, P.E., Schaaf, C.B., Sun, Q., Li, J., Huang, H., Kovalskyy, V., 2016b. A general method to normalize Landsat reflectance data to nadir BRDF adjusted reflectance. Remote. Sens. Environ. 176, 255–271. https://doi.org/10.1016/j.rse.2016.01.023.

Roy, D.P., Kovalskyy, V., Zhang, H.K., Vermote, E.F., Yan, L., Kumar, S.S., Egorov, A., 2016a. Characterization of Landsat-7 to Landsat-8 reflective wavelength and normalized difference vegetation index continuity. Remote. Sens. Environ. 185, 57–70. https://doi.org/10.1016/j.rse.2015.12.024.

Safanelli, J.L., Poppiel, R., Ruiz, L., Bonfatti, B., Mello, F., Rizzo, R., Demattê, J., 2020. Terrain Analysis in Google Earth Engine: A Method Adapted for High-Performance Global-Scale Analysis. ISPRS Int. J. Geoinf. 9, 400. https://doi.org/10.3390/ijgi9060400.

Sousa, G.P.B., de, Bellinaso, H., Rosas, J.T.F., Mello, D.C., de, Rosin, N.A., Amorim, M.T.A., dos Anjos Bartsch, B., Cardoso, M.C., Mallah, S., Francelino, M.R., Falcioni, R., Alves, M.R., Demattê, J.A.M., 2024. Assessing soil degradation in Brazilian agriculture by a remote sensing approach to monitor bare soil frequency: impact on soil carbon. Soil. Adv. 2, 100011. https://doi.org/10.1016/j.soilad.2024.100011.

Stockmann, U., Adams, M.A., Crawford, J.W., Field, D.J., Henakaarchchi, N., Jenkins, M., Minasny, B., McBratney, A.B., Courcelles, V. de R. de, Singh, K., Wheeler, I., Abbott, L., Angers, D.A., Baldock, J., Bird, M., Brookes, P.C., Chenu, C., Jastrow, J.D., Lal, R., Lehmann, J., O'Donnell, A.G., Parton, W.J., Whitehead, D., Zimmermann, M., 2013. The knowns, known unknowns and unknowns of sequestration of soil organic carbon. Agric. Ecosyst. Environ. 164, 80–99. https://doi.org/10.1016/j.agee.2012.10.001.

Szatmári, G., Pirkó, B., Koós, S., Laborczi, A., Bakacsi, Z., Szabó, J., Pásztor, L., 2019. Spatio-temporal assessment of topsoil organic carbon stock change in Hungary. Soil. Tillage Res. 195, 104410. https://doi.org/10.1016/j.still.2019.104410.

Tayebi, M., Fim Rosas, J.T., Mendes, W., de, S., Poppiel, R.R., Ostovari, Y., Ruiz, L.F.C., dos Santos, N.V., Cerri, C.E.P., Silva, S.H.G., Curi, N., Silvero, N.E.Q., Demattê, J.A.M., 2021. Drivers of Organic Carbon Stocks in Different LULC History and along Soil Depth for a 30 Years Image Time Series. Remote. Sens. (Basel) 13, 2223. https://doi.org/10.3390/rs13112223.

Tran, D.X., Dominati, E., Lowry, J., Mackay, A., Vibart, R., Pearson, D., Devantier, B., Noakes, E., 2024. Effects of spatial data resolution on the modelling and mapping of soil organic carbon content in hill country grassland landscapes. Soil. Use Manag. 40. https://doi.org/10.1111/sum.12966.

Ugbaje, S.U., Karunaratne, S., Bishop, T., Gregory, L., Searle, R., Coelli, K., Farrell, M., 2024. Space-time mapping of soil organic carbon stock and its local drivers: Potential for use in carbon accounting. Geoderma 441, 116771. https://doi.org/10.1016/j.geoderma.2023.116771.

Walkley, A., Black, I.A., 1934. An examination of the degtjareff method for determining soil organic matter, and a proposed modification of the chromic acid titration method. Soil. Sci. https://doi.org/10.1097/00010694-193401000-00003.

Wang, B., Gray, J.M., Waters, C.M., Rajin Anwar, M., Orgill, S.E., Cowie, A.L., Feng, P., Li Liu, D., 2022. Modelling and mapping soil organic carbon stocks under future climate change in south-eastern Australia. Geoderma 405, 115442. https://doi.org/10.1016/j.geoderma.2021.115442.

Wiesmeier, M., Urbanski, L., Hobley, E., Lang, B., von Lützow, M., Marin-Spiotta, E., van Wesemael, B., Rabot, E., Ließ, M., Garcia-Franco, N., Wollschläger, U., Vogel, H.-J., Kögel-Knabner, I., 2019. Soil organic carbon storage as a key function of soils - A review of drivers and indicators at various scales. Geoderma 333, 149–162. https://doi.org/10.1016/j.geoderma.2018.07.026.

Yigini, Y., Panagos, P., 2016. Assessment of soil organic carbon stocks under future climate and land cover changes in Europe. Sci. Total. Environ. 557558 838–850. https://doi.org/10.1016/j.scitotenv.2016.03.085.

Zhang, W., Zhang, X., Wu, W., Liu, H., 2024. The spatial variability of temporal changes in soil organic carbon and its drivers in a mountainous agricultural region of China. Catena (Amst. ) 246, 108402. https://doi.org/10.1016/j.catena.2024.108402.

Zhou, Y., Chartin, C., Van Oost, K., van Wesemael, B., 2022. High-resolution soil organic carbon mapping at the field scale in Southern Belgium (Wallonia). Geoderma 422, 115929. https://doi.org/10.1016/j.geoderma.2022.115929.